



## Phase diagrams for alkali-activated slag binders



Rupert J. Myers<sup>a,b,c,\*</sup>, Susan A. Bernal<sup>c,d</sup>, John L. Provis<sup>c</sup>

<sup>a</sup> Yale School of Forestry & Environmental Studies, Yale University, 195 Prospect St, New Haven 06511, CT, United States

<sup>b</sup> Department of Civil and Environmental Engineering, The University of California, Berkeley, Davis Hall, Berkeley 94720, CA, United States

<sup>c</sup> Department of Materials Science and Engineering, The University of Sheffield, Sir Robert Hadfield Building, Mappin St, Sheffield S1 3JD, United Kingdom

<sup>d</sup> Department of Civil and Structural Engineering, The University of Sheffield, Sir Frederick Mappin Building, Mappin St, Sheffield S1 3JD, United Kingdom

### ARTICLE INFO

#### Article history:

Received 12 September 2016

Received in revised form 30 December 2016

Accepted 10 February 2017

Available online 28 February 2017

#### Keywords:

Alkali activated cement

Granulated blast-furnace slag

Calcium-silicate-hydrate (C-S-H)

Hydration products

Thermodynamic calculations

### ABSTRACT

Phase diagrams for alkali-activated slag (AAS) binders are simulated at (metastable) thermodynamic equilibrium, spanning the relevant compositional envelopes for these materials. The phase diagrams are generally consistent with experimental observations in the literature, dominated by calcium (alkali) aluminosilicate hydrate (C-(N-)A-S-H) gels and Mg-Al layered double hydroxides. Relationships between the stabilities of the predicted solid phase assemblages, pore solution compositions, and the bulk chemical composition are identified, yielding an improved understanding of AAS binder chemistry. Strätlingite is predicted at low to intermediate Si concentrations and at high Al content, while zeolites (and thus most likely also disordered alkali-aluminosilicate (hydrate) gels) tend to precipitate at higher concentrations of both Si and Al; katoite and AFm-type phases are stabilised at intermediate levels of CaO + Al<sub>2</sub>O<sub>3</sub> + MgO. The application of these results in designing AAS binders can enable the phase assemblages and chemical properties of these materials to be more precisely controlled.

© 2017 The Authors. Published by Elsevier Ltd. This is an open access article under the CC BY-NC-ND license (<http://creativecommons.org/licenses/by-nc-nd/4.0/>).

### 1. Introduction

Alkali-activated slag (AAS) is a class of binder which is produced via the chemical reaction between an ‘activator’ (alkaline solution), e.g., NaOH (NH),<sup>1</sup> Na<sub>2</sub>SiO<sub>3</sub> (NS), Na<sub>2</sub>Si<sub>2</sub>O<sub>5</sub> (NS<sub>2</sub>), Na<sub>2</sub>CO<sub>3</sub> (N $\bar{C}$ ), or Na<sub>2</sub>SO<sub>4</sub> (N $\bar{S}$ ), and a metallurgical slag precursor, typically ground granulated blast furnace slag (BFS). These materials have been used in concrete infrastructure for several decades [1–3], particularly in areas where slag availability is high and a history of technical know-how exists, e.g. China and eastern Europe [2]. AAS can also be produced using other metallurgical slags that are less well utilised than BFS (e.g., phosphorus, copper, and steel slags [4]), bringing particularly high value in some specialised applications [5].

The chemistry of NH- and NS-activated slags is relatively well understood [2,6–13], with one of the key remaining questions concerning their resistance to carbonation, which is controlled to a significant extent by binder chemistry. For example, the carbonation resistance of sodium silicate-activated slag has been demonstrated to improve significantly as a function of bulk MgO content [14], although the stabilities of the Mg-Al layered double hydroxide (LDH) phases formed in

these materials need to be better understood to clarify their role in the underlying chemical mechanisms of carbonation [11]. The other typical solid reaction products in these binders are poorly-crystalline calcium(-sodium) aluminosilicate hydrate (C-(N-)A-S-H) gel [6, 10] and the ‘alumino-ferrite-mono’ (AFm) family of Ca-Al LDH phases [8], including strätlingite [15], and sodium aluminosilicate (hydrate) (N-A-S(-H))-type gels [6,11].

Compared to binders activated by silicates or hydroxides, significantly less research effort has been devoted to N $\bar{C}$ - and N $\bar{S}$ -activated slag binders, and consequently a better understanding of these binders is needed to enable them to be designed for improved performance, particularly with respect to setting characteristics and long-term chemical durability [16–18]. The solid phase assemblage in N $\bar{C}$ -activated slag normally contains poorly-crystalline C-(N-)A-S-H and N-A-S(-H) gels, Mg-Al LDH, and AFm-type phases predominantly intercalated with carbonate and/or hydroxide, e.g., hydrotalcite-like LDH (M<sub>4</sub>A $\bar{C}$ H<sub>9</sub>) and calcium monocarboaluminate hydrate (C<sub>4</sub>A $\bar{C}$ H<sub>11</sub>), and zeolites [16,17]. The carbonate-bearing phases typically present in these materials include calcite, aragonite and vaterite (C $\bar{C}$ ), gaylussite (N $\bar{C}$ C<sub>2</sub>H<sub>5</sub>) as a transient phase at early age, and thermonatrite (N $\bar{C}$ H) [16,17]. Typical solid reaction products in NS-activated slag binders include ettringite (C<sub>6</sub>A $\bar{S}$ <sub>3</sub>H<sub>32</sub>), AFm intercalated with  $\bar{S}$  (calcium monosulfoaluminate hydrate, C<sub>4</sub>A $\bar{S}$ H<sub>x</sub> with  $x \approx 12$  [19]), and gypsum (C $\bar{S}$ H<sub>2</sub>), although the abundances of these phases change significantly as a function of the slag chemical composition [20].

\* Corresponding author at: Yale School of Forestry & Environmental Studies, Yale University, 195 Prospect St, New Haven 06511, CT, United States.

E-mail addresses: [rupert.myers@gmail.com](mailto:rupert.myers@gmail.com) (R.J. Myers), [j.provis@sheffield.ac.uk](mailto:j.provis@sheffield.ac.uk) (J.L. Provis).

<sup>1</sup> Cement chemistry notation is used throughout the paper: C = CaO; S = SiO<sub>2</sub>; A = Al<sub>2</sub>O<sub>3</sub>; N = Na<sub>2</sub>O; M = MgO;  $\bar{C}$  = CO<sub>2</sub>;  $\bar{S}$  = SO<sub>3</sub>; H = H<sub>2</sub>O.

Recent research has substantially advanced the degree of confidence in which the solid phase assemblages of AAS binders can be accurately predicted under (metastable) thermodynamic equilibrium conditions. Notably, the CNASH<sub>ss</sub> thermodynamic model [21], containing the first explicit descriptions of Al and alkali uptake in C-S-H-type phases, describes the volumetric properties of C-(N-)A-S-H gel in AAS binders, and was validated against a large set of solubility data in the CaO-(Na<sub>2</sub>O,Al<sub>2</sub>O<sub>3</sub>)-SiO<sub>2</sub>-H<sub>2</sub>O systems, C-(A-)S-H gel chemical compositions, and NH- and NS-activated slag pore solution chemistry. The CNASH<sub>ss</sub> thermodynamic model was later applied to simulate the chemistry of NS- and N $\bar{C}$ -activated slag binders [11,22]; simulation of the former system showed a relatively lower stability of ettringite than existing thermodynamic modelling work [23], in closer agreement with the experimental literature, and that zeolite-type phases are also potentially stable in these systems. An ideal solid solution model for Mg-Al LDH intercalated with OH<sup>-</sup> (hereafter termed MA-OH-LDH) was also developed, again providing a significant advancement over earlier work [24, 25], which has further improved the utility of thermodynamic modelling to predict AAS binder chemistry.

In this paper, the solid phase assemblages in NS-, NS<sub>2</sub>-, N $\bar{C}$ - and N $\bar{S}$ -activated slag binders are predicted by thermodynamic modelling, and presented as phase diagrams in the CaO-Al<sub>2</sub>O<sub>3</sub>-MgO pseudo-ternary system at fixed contents of SiO<sub>2</sub>, sulfur, and Na<sub>2</sub>O, extending from recently published phase diagrams for NH-AS [11]. These phase diagrams are compared to experimental results to assess the reliability of the simulations, to gain insight into kinetic and other thermodynamic effects not captured by the modelling performed, and to improve the current understanding of AAS binder chemistry across a wide range of activator chemistries.

## 2. Methods

Phase diagrams for NS-, NS<sub>2</sub>-, N $\bar{C}$ -, and N $\bar{S}$ -activated slag binders were generated using simulated slag precursors with 30 wt% and 40 wt% SiO<sub>2</sub>, and 2 wt% SO<sub>3</sub> equivalent as H<sub>2</sub>S (i.e., specified as S<sup>2-</sup> and H<sup>+</sup>), to approximate the typical chemical composition of BFS [26,27]. The remainders of the chemical compositions of the slag precursors were varied within the CaO-Al<sub>2</sub>O<sub>3</sub>-MgO pseudo-ternary system to span the range of chemistries that are relevant to AAS-based binders: 0.5 ≤ CaO ≤ 1, 0 ≤ Al<sub>2</sub>O<sub>3</sub> ≤ 0.5 and 0 ≤ MgO ≤ 0.5 (on a molar basis), on the basis of the sum of CaO + Al<sub>2</sub>O<sub>3</sub> + MgO being normalised to 1 (i.e., at fixed contents of SiO<sub>2</sub> and SO<sub>3</sub> equivalent, which are thus omitted from the pseudo-ternary diagrams). Fe was excluded from the simulations, consistent with the identification of its passivated state as entrained metallic particles in BFS [28], and with sulfur in the slag represented as sulfide. Therefore, the simulations are most relevant to AAS synthesised using BFS and less to those produced using non-ferrous slags, e.g., Cu slag (typically having compositions in the CaO-FeO-Fe<sub>2</sub>O<sub>3</sub>-SiO<sub>2</sub> system). A slag reaction extent of 60% was specified, which lies in the normal range measured for AAS binders after 180 days of reaction [6,7,14,17]. Therefore, simulations were carried out using 100 g slag, 60 g of which is 'reactive' and comprised of CaO, Al<sub>2</sub>O<sub>3</sub>, MgO, SiO<sub>2</sub>, S<sup>2-</sup>, and H<sup>+</sup> (for charge balance), and 40 g of which is 'unreactive'. A water to binder (solids + anhydrous activator component) mass ratio (w/b) of 0.4 was used, which is typical for AAS binders. A dosage of 8 g activator per 100 g slag was specified except for the Na<sub>2</sub>O·2SiO<sub>2</sub> (NS<sub>2</sub>) activator, which was added at a dose of 4 g Na<sub>2</sub>O per 100 g slag.

Thermodynamic modelling was performed using the Gibbs energy minimisation software GEM-Selektor v.3 (<http://gems.web.psi.ch/>) [29, 30] using the thermodynamic database described in [11], which is based on an updated version of CEMDATA07 [24]. This thermodynamic database contains ideal solid solution models for C-(N-)A-S-H gel [21] and MA-OH-LDH [11]. These models are provided as Supporting Information in formats that can be directly loaded into GEMS v.3.2 and v.3.3. The thermodynamic database also contains a small subset of zeolites. These zeolites were chosen following a preliminary investigation which showed that thermodynamic modelling results obtained using these

data are consistent with experimentally determined phase assemblages of AAS binders. The thermodynamic data used to describe the zeolite phases and alkali carbonate minerals here should be treated as provisional because they were not recompiled for full internal consistency with the thermodynamic database used [11]. These data and the thermodynamic model used to describe MA-OH-LDH are based on data with generally larger uncertainty than that associated with the solubility data used to describe the other solid phases here. Therefore, the modelled stability regions for these phases should be regarded as less reliable than the others.

It should also be noted that this thermodynamic database does not contain data for magnesium-silicate-hydrate (M-S-H) phases that can stabilise in high Mg cementitious and clay-containing environments [31], which thus reduces the reliability of the Mg-rich regions of the phase diagrams modelled here. These M-S-H phases have not yet been identified in AAS binders, and data for these phases have only very recently been published [32]. Further work is needed to understand their compatibility in AAS systems (including consideration of kinetic effects). Precipitation of Si-hydrogarnet was suppressed because this phase tends not to form at ambient temperature and pressure in hydrated cementitious systems [24]. A predominantly N<sub>2</sub> (g) atmosphere was used as the gas phase in all simulations.

The Truesdell-Jones form of the extended Debye-Hückel equation (Eq. (1)) [33] and the ideal gas equation of state were used as aqueous and gaseous phase models, respectively, with the average ion size ( $\bar{a}$ , Å) and the parameter for common short-range interactions of charged species ( $b_\gamma$ , kg mol<sup>-1</sup>) specified to represent NaOH-dominated solutions (3.31 Å and 0.098 kg mol<sup>-1</sup>, respectively [33]).

$$\log_{10} \gamma_j = \frac{-A_\gamma z_j^2 \sqrt{I}}{1 + \bar{a} B_\gamma \sqrt{I}} + b_\gamma I + \log_{10} \frac{x_{jw}}{X_w} \quad (1)$$

The parameters  $\gamma_j$  and  $z_j$  in Eq. (1) are the activity coefficient and charge of the  $j$ th aqueous species, respectively;  $A_\gamma$  (kg<sup>0.5</sup> mol<sup>-0.5</sup>) and  $B_\gamma$  (kg<sup>0.5</sup> mol<sup>-0.5</sup> cm<sup>-1</sup>) are T,P-dependent electrostatic parameters;  $I$  is the ionic strength of the aqueous electrolyte phase (mol kg<sup>-1</sup>);  $x_{jw}$  (mol) is the molar quantity of water; and  $X_w$  (mol) is the total molar amount of the aqueous phase. The activity of water is calculated from the osmotic coefficient [33], and unity activity coefficients are used for neutral dissolved species.

A step size of 0.02 normalised CaO-Al<sub>2</sub>O<sub>3</sub>-MgO molar composition units was used to construct the phase diagrams, i.e., (CaO, Al<sub>2</sub>O<sub>3</sub>, MgO) = (0.00, 1.00, 0.00), (0.02, 0.98, 0.00), (0.02, 0.96, 0.02), and so on. The masses of each stable solid phase and the chemical compositions of the aqueous solutions simulated by GEMS were transferred to Origin and plotted. Stability regions for each phase correspond to the chemical composition envelopes where they are simulated to have non-zero mass. Major, minor, and trace classifications are assigned to solid phases with masses of >40%, 5–40%, and <5% of the total simulated solid mass, respectively. The full set of modelled solid (tabulated) and aqueous (tabulated and graphical) phase data reported here are presented as Supporting Information. Additional properties of the C-(N-)A-S-H gel phases simulated using the CNASH<sub>ss</sub> thermodynamic model, its chemical composition, density, molar volume, and mean chain length (calculated using formula for non-cross-linked C-(N-)A-S-H structures and described in [21,34]), are provided alongside those data (Supporting Information).

## 3. Results and discussion

### 3.1. Phase diagrams for NS-activated slag binders

The simulated phase diagrams for NS-activated slag binders (Fig. 1; in this graphic and other similar graphics throughout the paper, the table of compositional regions refers to both parts A and B) are dominated by C-(N-)A-S-H gel and Mg-Al LDH intercalated with

Region	Simulated solid phase assemblage										
	1	2	3	4	5	6	7	8	9	10	11
a	X	-	-	-	-	-	-	-	MT	MT	-
b	X	-	-	-	-	-	-	-	-	M	-
c	X	-	-	-	T	-	-	-	MT	MT	-
d	X	-	-	-	T	-	-	-	-	M	-
e	X	-	-	-	T	M	-	-	M	-	-
f	X	-	-	-	T	M	-	-	MT	MT	-
g	X	MT	-	-	MT	-	-	-	-	MT	-
h	X	MT	-	-	MT	MT	-	-	-	MT	-
i	X	MT	-	-	T	-	-	-	MT	MT	-
j	X	MT	-	-	T	M	-	-	MT	-	-
k	X	MT	-	MT	T	M	-	-	T	-	-
l	X	MT	-	MT	T	M	-	-	-	-	-
m	X	M	-	-	M	-	-	-	-	-	-
n	X	M	-	-	MT	MT	-	-	-	-	-
o	X	MT	MT	MT	T	M	-	-	-	-	-
p	X	M	-	-	M	-	-	-	-	-	-
q	X	M	T	-	M	-	-	-	-	-	-
r	X	MT	XMT	-	MT	MT	-	-	-	-	-
s	XM	MT	XMT	-	MT	MT	-	-	-	-	-
t	XM	MT	XMT	-	MT	-	MT	-	-	-	-
u	MT	MT	XMT	-	M	-	M	T	-	-	-
v	-	MT	X	-	M	-	M	MT	-	-	-
w	-	MT	X	-	M	-	M	MT	-	-	MT
x	X	-	-	-	-	-	-	-	-	-	-
y	X	-	-	-	-	-	-	-	MT	MT	-
z	X	-	-	-	-	-	-	-	M	-	-
aa	X	-	-	-	T	-	-	-	MT	-	-
ab	X	-	-	-	MT	-	-	-	-	MT	-
ac	X	-	-	-	T	-	-	-	T	T	-
ad	X	-	-	-	M	-	-	-	-	-	-
ae	X	MT	-	-	MT	-	-	-	MT	MT	-
af	X	MT	-	-	MT	-	-	-	-	MT	-
ag	X	MT	-	-	M	-	-	-	-	-	-
ah	X	M	-	-	MT	-	-	-	MT	-	-
ai	X	MT	MT	-	M	-	-	-	-	-	-
aj	XM	M	-	-	MT	-	MT	MT	-	-	-
ak	X	M	-	-	M	-	MT	-	-	-	-
al	X	MT	MT	-	M	-	MT	-	-	-	-
am	XMT	MT	XMT	-	M	-	M	MT	-	-	-
an	-	MT	XM	-	M	-	M	M	-	-	-
ao	-	MT	XM	-	M	-	M	M	-	-	MT

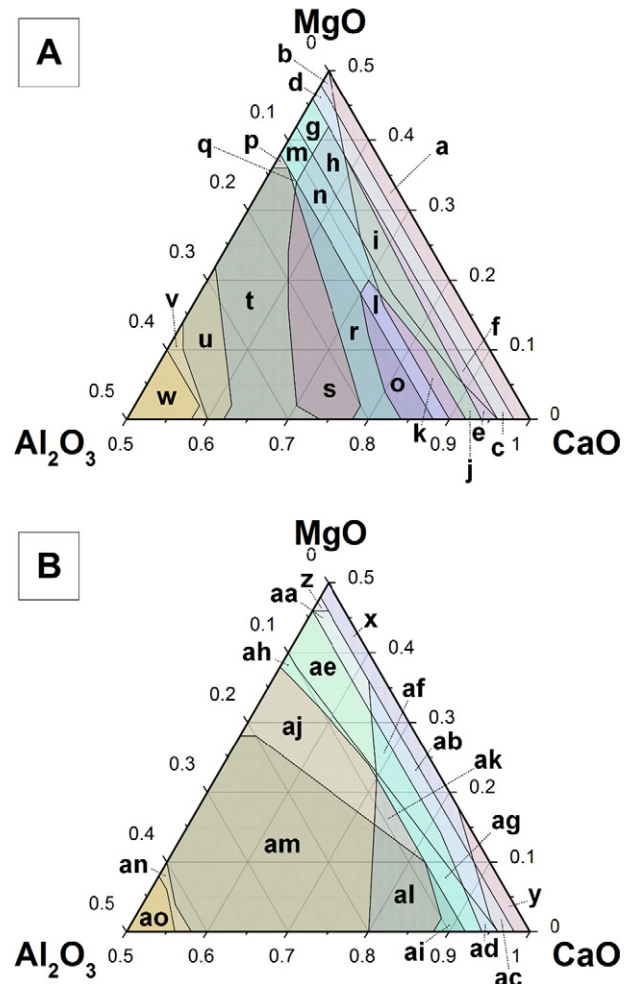


Fig. 1. Phase diagrams in the CaO-Al<sub>2</sub>O<sub>3</sub>-MgO chemical system for NS-activated slag-based binders derived from BFS containing sulfide at a molar equivalent to 2 wt% SO<sub>3</sub>, and A) 30 wt% SiO<sub>2</sub> or B) 40 wt% SiO<sub>2</sub>. The w/b ratio is 0.4, the slag reaction extent is 60%, and the units are in mol fraction. The simulated solid phases are: 1, CNASH<sub>ss</sub>; 2, MA-OH-LDH<sub>ss</sub>; 3, strätlingite; 4, katoite; 5, ettringite; 6, C<sub>4</sub>A $\bar{S}$ H<sub>ss</sub>; 7, natrolite; 8, Ca-heulandite; 9, portlandite; 10, brucite; 11, AH<sub>3</sub> (mc). Solid phases are classified by quantity, with major, minor, and trace phases denoted in the legend by X, M, and T, respectively. Multiple letters are used where more than one category applies.

OH<sup>-</sup> (represented by the CNASH<sub>ss</sub> and MA-OH-LDH<sub>ss</sub> ideal solid solution models, respectively [11]). These phases occur across the full composition range analysed, except under the most Al-rich conditions (Al<sub>2</sub>O<sub>3</sub>/(CaO + Al<sub>2</sub>O<sub>3</sub> + MgO) > ~0.4; regions *u* and *v* in Fig. 1A, and *an* and *ao* in Fig. 1B), where C-(N-)A-S-H gel is absent, and in highly Al-deficient chemistries (Al<sub>2</sub>O<sub>3</sub>/(CaO + Al<sub>2</sub>O<sub>3</sub> + MgO) < ~0.05; regions *a-f* in Fig. 1A, and regions *x-ad* in Fig. 1B), where there is insufficient Al available to form MA-OH-LDH.

Ettringite is predicted to precipitate in minor or trace amounts in a similar chemical compositional envelope to MA-OH-LDH (Al<sub>2</sub>O<sub>3</sub>/(CaO + Al<sub>2</sub>O<sub>3</sub> + MgO) < ~0.05), demonstrating that it is thermodynamically feasible to form this phase in NS-activated slag binders with a bulk raw material sulfur content equivalent to 2 wt% SO<sub>3</sub>. Ettringite is not typically observed as a reaction product in NS-activated slag binders despite BFS normally having similar sulfur concentrations to the value used here [7,14]. This result may be partly explained if a significant proportion of sulfur in the binder adsorbs to reaction products rather than being free in the bulk aqueous phase (and thus available to precipitate as ettringite). This would be somewhat consistent with the reported tendency for C-S-H-type phases to adsorb aqueous sulfate [35,36], and the intercalation of  $\bar{S}$  in Mg-Al LDH, which is reported although not fully understood [37]. The discrepancy between the prediction of trace and minor quantities of C<sub>4</sub>A $\bar{S}$ H<sub>12</sub> here (depicted as C<sub>4</sub>A $\bar{S}$ H<sub>ss</sub>, a non-ideal solid solution between C<sub>4</sub>A $\bar{S}$ H<sub>12</sub> and C<sub>4</sub>A $\bar{S}$ H<sub>13</sub> [38]), which is stable at intermediate Ca and Al concentrations and relatively weakly

dependent on the Mg content, and the absence of this phase from experimental data for NS-activated slag binders with bulk raw material sulfur concentrations similar to that used in the simulations [7,14], may be explained similarly. The different redox conditions of the simulated (oxidised) and experimental (reduced) sulfur speciation in NS-activated slag binders [7,14] (with limited air exposure) may also contribute significantly to the identified discrepancy in the precipitated  $\bar{S}$ -containing solid phases, particularly because adsorption phenomena depend greatly on redox chemistry [39].

Several additional minor and trace solid phases are simulated in NS-activated slag binders within the chemical composition range analysed. Portlandite is only simulated at low Al content and its stability field shrinks greatly as a function of increasing SiO<sub>2</sub> concentration, (Al<sub>2</sub>O<sub>3</sub>/(CaO + Al<sub>2</sub>O<sub>3</sub> + MgO) < ~0.1) for slag with bulk SiO<sub>2</sub> = 30 wt% (Fig. 1A), and only near the CaO corner of the pseudo-ternary system (regions *y* and *ac*) for raw materials with bulk SiO<sub>2</sub> = 40 wt% (Fig. 1B). The prediction of portlandite here is partly attributed to the CNASH<sub>ss</sub> thermodynamic model overestimating the solubility of Ca in equilibrium with C-(N-)A-S-H gel at Ca/Si > 1.3, which would lead to superficially higher aqueous Ca concentrations and the relative stability of portlandite in this chemical composition range. Nonetheless, portlandite would in any case be stable in some regions with relatively high Ca concentrations (bulk Ca/Si molar ratios > 1.5), e.g., at the bottom right corner of region *a* (Fig. 1A). Therefore, the simulated stability fields of portlandite should be marginally reduced in favour of C-(N-)A-S-H

gel, but are otherwise reliable. Brucite is predicted under Al-deficient conditions, and its relative stability increases to higher Al concentrations in the presence of more Mg: from  $Al_2O_3/(CaO + Al_2O_3 + MgO) < \sim 0.05$  at low Mg content to  $Al_2O_3/(CaO + Al_2O_3 + MgO) < \sim 0.1$  at high Mg content.  $AH_3_{(mc)}$  is only simulated at the most Al-rich compositions ( $Al_2O_3/(CaO + Al_2O_3 + MgO) > \sim 0.4$ ). The stability field of  $AH_3_{(mc)}$  shrinks to slightly more Al-rich compositions in the system with higher  $SiO_2$  content. These phases are not generally observed in experimental studies of NS-activated slag binders because these binders typically contain intermediate concentrations of all three oxide components.

Strätlingite and katoite are sometimes identified experimentally in NS-activated slag binders [14], with strätlingite particularly favoured in these materials when relatively Al-rich slags are used [15], which is captured in the simulated phase diagrams (Fig. 1). The stability field of strätlingite is generally only predicted at  $Al_2O_3/(CaO + Al_2O_3 + MgO) > \sim 0.1$  but includes slightly more Ca-rich and less Mg-rich compositions in the phase diagram simulated using the higher  $SiO_2$  content of 40 wt%. Recent experimental work has shown that strätlingite is stable in the simulated composition regions at 20°C [40], in good agreement with the simulations. Katoite is only stable at intermediate CaO- $Al_2O_3$ -MgO compositions, and not at all in the 40 wt%  $SiO_2$  system (Fig. 1B). This result is consistent with the identified occurrence of this phase in more Ca-rich systems: much stronger X-ray diffraction reflections for katoite are identified in NH-activated slag [9] than NS-activated slag [14] binders, and katoite/

hydrogarnet-type phases have been postulated to exist in hydrated 75 wt% BFS/25 wt% Portland cement blends [41].

The stabilities of the two stable zeolite phases present in Fig. 1, natrolite and Ca-heulandite (which are present in minor and trace quantities), increase with the bulk  $SiO_2$  content of the raw materials; these phases are less stable at lower Al and Ca concentrations. The prediction of zeolites in the phase diagrams, and the large composition ranges in which these phases are predicted to be stable, indicates that they are likely to form in binders such as NS-activated slag with moderate to high Al content: zeolites [14] and zeolite-like phases such as N-A-S(-H) gels [6,34] have been identified in these materials, in good agreement with these results. The more Al-rich and less Ca-rich compositions needed to form these phases would also be approached in hybrid alkali-activated systems produced using BFS and e.g., metakaolin. Natrolite is predicted to be relatively more stable than Ca-heulandite, although this trend may be influenced by the relatively lower level of confidence assigned to the thermodynamic data for zeolites used here relative to the other phases simulated (Section 2 and [11]).

3.2. Phase diagrams for  $NS_2$ -activated slag binders

The phase diagrams simulated for NS- and  $NS_2$ -activated slag binders (Fig. 1 and Fig. 2, respectively) contain the same solid phases but in moderately different stability regions. Less katoite and  $C_4ASH_{12}$

Region	Simulated solid phase assemblage										
	1	2	3	4	5	6	7	8	9	10	11
a	X	-	-	-	-	-	-	-	-	M	-
b	X	-	-	-	-	-	-	-	MT	MT	-
c	X	-	-	-	T	-	-	-	-	M	-
d	X	-	-	-	T	-	-	-	MT	MT	-
e	X	-	-	-	T	T	-	-	M	T	-
f	X	-	-	-	T	T	-	-	M	-	-
g	X	T	-	-	MT	MT	-	-	MT	MT	-
h	X	MT	-	-	MT	-	-	-	-	MT	-
i	X	MT	-	-	M	MT	-	-	-	MT	-
j	X	MT	-	-	MT	MT	-	-	MT	-	-
k	X	M	-	-	M	MT	-	-	-	-	-
l	X	T	-	T	MT	M	-	-	-	-	-
m	X	T	T	T	MT	M	-	-	-	-	-
n	X	M	-	-	M	-	-	T	-	-	-
o	X	M	-	-	MT	-	-	-	-	-	-
p	X	MT	MT	-	MT	MT	-	-	-	-	-
q	X	MT	MT	-	MT	-	-	-	-	-	-
r	X	M	-	-	MT	-	MT	T	-	-	-
s	X	M	-	-	MT	-	MT	-	-	-	-
t	XM	MT	XMT	-	-	-	MT	-	-	-	-
u	XMT	MT	XMT	-	-	-	M	MT	-	-	-
v	-	MT	X	-	-	-	M	M	-	-	-
w	-	T	X	-	-	-	M	M	-	-	MT
x	X	-	-	-	-	-	-	-	-	MT	-
y	X	-	-	-	-	-	-	-	-	M	-
z	X	-	-	-	MT	-	-	-	-	MT	-
aa	X	-	-	-	T	-	-	MT	-	M	-
ab	X	T	-	-	MT	-	-	-	-	T	-
ac	X	MT	-	-	M	-	-	-	-	-	-
ad	X	-	-	-	M	-	-	-	-	-	-
ae	X	MT	-	-	MT	-	-	MT	-	MT	-
af	X	M	-	-	MT	-	-	MT	-	-	-
ag	X	MT	-	-	M	-	T	-	-	-	-
ah	X	T	T	-	M	-	MT	-	-	-	-
ai	XM	MT	-	-	M	-	MT	MT	-	-	-
aj	XMT	MT	MT	-	M	-	M	MT	-	-	-
ak	-	T	XM	-	M	-	M	M	-	-	-

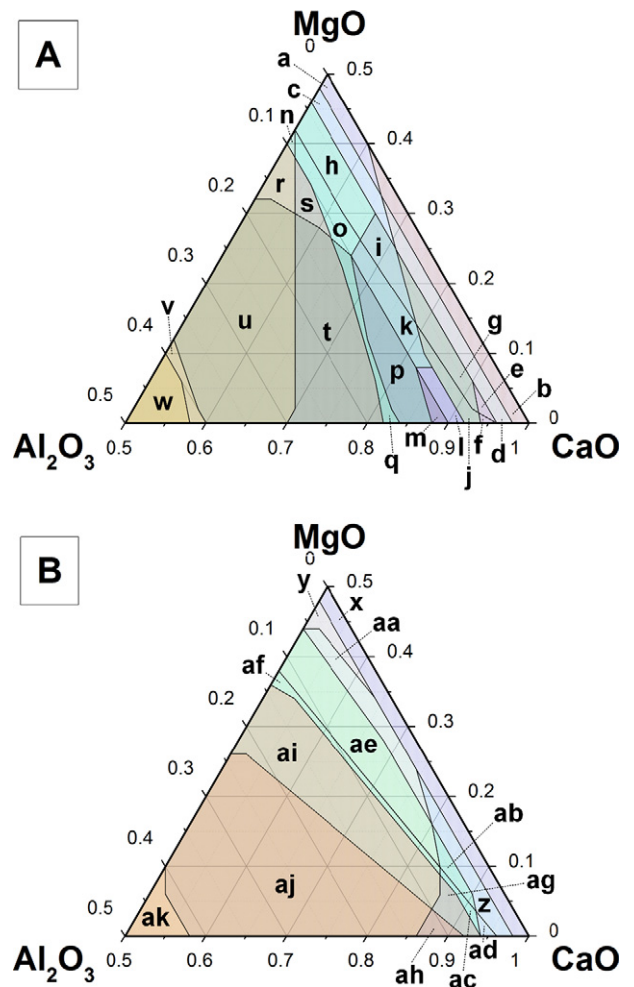


Fig. 2. Phase diagrams in the CaO- $Al_2O_3$ -MgO chemical system for  $NS_2$ -activated slag binders derived from BFS with sulfide at a molar equivalent to 2 wt%  $SO_3$ , and A) 30 wt%  $SiO_2$  or B) 40 wt%  $SiO_2$ . The w/b ratio is 0.4, the slag reaction extent is 60%, and the units are in mol fraction. The simulated solid phases are: 1, CNASH<sub>ss</sub>; 2, MA-OH-LDH<sub>ss</sub>; 3, strätlingite; 4, katoite; 5, ettringite; 6,  $C_4ASH_{ss}$ ; 7, natrolite; 8, Ca-heulandite; 9, portlandite; 10, brucite; 11,  $AH_3_{(mc)}$ . Solid phases are classified by quantity, with major, minor, and trace phases denoted in the legend by X, M, and T, respectively. Multiple letters are used where more than one category applies.

are simulated with NS<sub>2</sub> activation (Fig. 2), consistent with the predicted relatively lower stabilities of these phases as a function of increasing Si content (Fig. 1). The stability fields of portlandite are similarly narrowed (Fig. 2A) or absent (Fig. 2B) in the phase diagrams simulated for NS<sub>2</sub>-activated slag binders relative to the more Ca-rich NS-activated slag systems. AH<sub>3</sub> (mc) is stable in both systems. C-(N-)A-S-H gel is predicted to stabilise over almost the full range of modelled chemical compositions in the phase diagrams for NS<sub>2</sub>-activated slag binders, again with the exception of the most Al-rich compositions ( $\text{Al}_2\text{O}_3/(\text{CaO} + \text{Al}_2\text{O}_3 + \text{MgO}) > \sim 0.4$ ; regions *v* and *w* in Fig. 2A, and *ak* in Fig. 2B).

Etringite is simulated in minor or trace amounts in the phase diagrams for NS<sub>2</sub>-activated slag binders, and is stable over essentially the full modelled CaO-Al<sub>2</sub>O<sub>3</sub>-MgO composition range. Its absence from experimental NS<sub>2</sub>-activated slag systems may again be explained by the significant adsorption of sulfate in predominantly C-S-H type gels [35, 36], which are the main reaction products observed experimentally in binders synthesised using BFS with NS<sub>2</sub>-composition sodium silicate activators [12,13,42,43].

Strätlingite is predicted to be present for  $\text{Al}_2\text{O}_3/(\text{CaO} + \text{Al}_2\text{O}_3 + \text{MgO}) > \sim 0.1$  in the phase diagram for NS<sub>2</sub>-activated slag binders produced using slag with 30 wt% SiO<sub>2</sub>. However, this phase is significantly less stable in the 40 wt% SiO<sub>2</sub> system, demonstrating that this phase is stabilised at relatively low to intermediate SiO<sub>2</sub> concentrations, and so it is not expected to precipitate in all sodium silicate-activated slag binders. It has been demonstrated that the occurrence of strätlingite in AAS binders is also greatly influenced by the bulk Al<sub>2</sub>O<sub>3</sub> content [11,15], as this phase acts as a sink for excess Al remaining beyond its capacity for incorporation in C-(N-)A-S-H gel and Mg-Al LDH phases. This observation is captured in the phase diagrams, which contain strätlingite in major quantities at the most Al-rich compositions. The stability fields of natrolite and Ca-heulandite expand to include relatively more Al-deficient compositions at higher Si concentrations such as the typical bulk chemical composition of NS<sub>2</sub>-activated slag binders, thus indicating that zeolite-type phases can be expected to precipitate in these binders. This result is consistent with the identification of gismondine by synchrotron-based X-ray diffractograms in NS<sub>2</sub>-activated slag binders at low MgO content [42]. It is also likely that poorly crystalline zeolite-like materials such as N-A-S(-H) gels precipitate in these binders [34], although a full set of thermodynamic data and models for this phase have not yet been published, preventing its inclusion in the modelling performed here.

The stability fields of MA-OH-LDH in the phase diagrams for NS- and NS<sub>2</sub>-activated slag binders are similar, which shows that the precipitation of this phase in these systems is weakly dependent on the bulk SiO<sub>2</sub> content in the simulated composition range [11] (i.e., using slags with 30–40 wt% SiO<sub>2</sub> with either NS or NS<sub>2</sub> activators; it is relatively immaterial whether additional Si is provided by the slag or by the activator). Together with the relative independence of the simulated low-Al MA-OH-LDH stability field boundaries with respect to the MgO content ( $\text{Al}_2\text{O}_3/(\text{CaO} + \text{Al}_2\text{O}_3 + \text{MgO}) < \sim 0.05$ ) for both NS- and NS<sub>2</sub>-activated slag binders (Figs. 1 and 2), the results presented here show that incorporation of Al into this phase is secondary to its uptake in C-(N-)A-S-H gel. Brucite is the stable Mg-containing phase at very low Al concentrations, with Al preferentially incorporated in C-(N-)A-S-H gel here. Brucite is predicted to form over a moderate range of compositions here, albeit in minor or trace quantities, that extend to more Al-rich compositions at higher Mg content, particularly in the 40 wt% SiO<sub>2</sub> system. The moderate stability of brucite here contrasts with the absence of this phase from essentially all experimentally-synthesised AAS binders [2,6–13,44,45], which most likely indicates that the MA-OH-LDH<sub>ss</sub> model, included in the thermodynamic database used here, is too soluble. It is unlikely that the error is in the thermodynamic data for brucite, because of the high confidence which exists regarding the accuracy of these data [46–49]. This issue is revisited in Section 3.5. The higher than expected stability of brucite here may also relate to the thermodynamic database used here lacking a description of M-S-H phases (Section 2).

### 3.3. Phase diagrams for $\overline{\text{NC}}$ -activated slag binders

Similar phases are simulated for  $\overline{\text{NC}}$ -activated slag binders (Fig. 3) as for the  $\overline{\text{C}}$ -free systems (Figs. 1–2), including CNASH<sub>ss</sub>, MA-OH-LDH<sub>ss</sub>, and strätlingite as the most dominant reaction products. CNASH<sub>ss</sub> is predicted throughout the compositional range of interest except at  $\text{Al}_2\text{O}_3/(\text{CaO} + \text{Al}_2\text{O}_3 + \text{MgO}) > \sim 0.3$ , and MA-OH-LDH<sub>ss</sub> is simulated in a similar compositional region excluding very low Al<sub>2</sub>O<sub>3</sub> content ( $\sim 0.1 < \text{Al}_2\text{O}_3/(\text{CaO} + \text{Al}_2\text{O}_3 + \text{MgO}) < \sim 0.35$ ). The issue of carbonate substitution into the MA-LDH phases is addressed in more detail below.

The presence of minor and trace quantities of ettringite in the simulated phase diagrams for the  $\overline{\text{NC}}$ -activated slag system demonstrates that it has not been replaced by the structurally-similar  $\text{C}_6\overline{\text{AC}}_3\text{H}_3\text{Z}_2$  phase in the stable assemblage, despite the high carbonate concentration supplied by the activator. The simulations conducted here do not include the possibility of solid solution between these phases, although this has been observed in the laboratory [50]. Calcium monocarboaluminate hydrate ( $\text{C}_4\overline{\text{ACH}}_{11}$ ) is preferentially stabilised over  $\text{C}_4\overline{\text{ASH}}_{ss}$ , which is not predicted to form in  $\overline{\text{NC}}$ -activated slag. Therefore, it is likely that the sulfate that would have been incorporated into  $\text{C}_4\overline{\text{ASH}}_{ss}$  is displaced by the excess carbonate present, by comparison to the NS-activated systems, and is instead used to precipitate ettringite. This result is consistent with the known stabilisation of ettringite and carboaluminates in preference to sulfate AFm phases in limestone-blended Portland cements [51]. The  $\text{C}_4\overline{\text{ACH}}_{11}$  phase is a major reaction product in the simulated  $\overline{\text{NC}}$ -activated slag system and is stable over a large range of CaO-Al<sub>2</sub>O<sub>3</sub>-MgO compositions for precursors with a bulk SiO<sub>2</sub> content of 30 wt%. However, its stability field is greatly decreased in the 40 wt% SiO<sub>2</sub> system, indicating that it is strongly destabilised as a function of increasing SiO<sub>2</sub> concentration in favour of natrolite and Ca-heulandite. Strätlingite is simulated in Al-rich compositions ( $\text{Al}_2\text{O}_3/(\text{CaO} + \text{Al}_2\text{O}_3 + \text{MgO}) > \sim 0.2$ ), which is consistent with its aforementioned (Section 3.2) stabilisation at relatively low to intermediate SiO<sub>2</sub> concentrations. AH<sub>3</sub> (mc) is also predicted in the most Al-rich composition region ( $\text{Al}_2\text{O}_3/(\text{CaO} + \text{Al}_2\text{O}_3 + \text{MgO}) > \sim 0.35$ ). Katoite is absent from the simulated phase diagrams for  $\overline{\text{NC}}$ -activated slag binders.

Calcite is present as a minor or trace reaction product over the full range of simulated chemical compositions in this  $\overline{\text{NC}}$ -activated slag system, which agrees closely with experimental results published for these materials [16,17]. The high stability of calcite here indicates that the relatively less stable aragonite and/or vaterite CaCO<sub>3</sub> polymorphs may also form in  $\overline{\text{NC}}$ -activated slag binders, which is experimentally observed [16,17,52]: the thermodynamic stabilities of these phases are similar ([11]), and their precipitation tends to be controlled by kinetics and by the nature of minor dissolved species [53].

The stability fields of natrolite and Ca-heulandite are predicted to occur over a wide range of CaO-Al<sub>2</sub>O<sub>3</sub>-MgO compositions and are enlarged in the  $\overline{\text{NC}}$ -activated slag binder system relative to the phase diagrams for NS-activated (Fig. 1) and NS<sub>2</sub>-activated slag binders (Fig. 2). Ca-heulandite is identified in X-ray diffractograms of  $\overline{\text{NC}}$ -activated slag binders at curing times  $\geq 7$  days [16], in close agreement with the modelling results, which also confers confidence in the thermodynamic data used here for this phase ([11]). This result indicates that N-A-S(-H)-type gels are more likely to form when using  $\overline{\text{NC}}$  as an alkali activator, than in NS- and NS<sub>2</sub>-activated slag binders. This is in agreement with <sup>29</sup>Si magic angle spinning nuclear magnetic resonance (MAS NMR) results for these carbonate-containing systems [17].

The carbonate-containing hydroxalite-like MA- $\overline{\text{C}}$ -LDH is only stable at very high Al concentrations ( $\text{Al}_2\text{O}_3/(\text{CaO} + \text{Al}_2\text{O}_3 + \text{MgO}) > \sim 0.35$ ), stabilising at the expense of MA-OH-LDH<sub>ss</sub> in this composition range. The overall lower stability predicted for this carbonate-containing Mg-

Region	Simulated solid phase assemblage													
	1	2	3	5	7	8	9	10	11	12	13	14		
a	X	-	-	-	-	-	MT	MT	-	-	-	-	MT	
b	X	-	-	-	-	-	-	M	-	-	-	-	MT	
c	X	-	-	T	-	-	MT	MT	-	MT	-	-	MT	
d	X	-	-	T	-	-	-	MT	-	MT	-	-	MT	
e	X	MT	-	T	-	-	-	MT	-	M	-	-	MT	
f	X	-	-	T	-	-	-	-	-	X	-	-	MT	
g	X	MT	-	T	-	-	-	-	-	XM	-	-	MT	
h	XM	MT	-	MT	MT	-	-	-	-	XM	-	-	MT	
i	MT	MT	MT	-	M	-	-	-	-	XM	-	-	MT	
j	-	-	M	-	M	-	-	-	-	M	-	-	MT	
k	-	-	M	-	M	-	-	-	-	M	-	-	MT	
l	-	T	M	-	M	-	-	-	-	M	-	-	MT	
m	-	-	M	-	M	-	-	-	-	M	MT	MT	MT	
n	-	-	XM	-	M	-	-	-	T	MT	MT	MT	MT	
o	-	-	M	-	M	-	-	-	MT	-	T	MT	MT	
p	X	-	-	-	-	-	-	M	-	-	-	-	M	
q	X	-	-	-	-	-	MT	MT	-	-	-	-	M	
r	X	-	-	-	-	-	-	M	-	-	-	-	M	
s	X	-	-	-	T	-	-	M	-	-	-	-	M	
t	X	T	-	-	-	T	-	M	-	-	-	-	M	
u	X	T	-	-	-	-	-	M	-	-	-	-	M	
v	X	T	-	-	-	-	-	M	-	-	-	-	M	
w	X	-	-	T	-	-	-	MT	-	-	-	-	M	
x	X	-	-	T	-	-	MT	MT	-	-	-	-	M	
y	X	-	-	T	-	-	-	MT	-	MT	-	-	M	
z	X	-	-	T	-	-	-	-	-	M	-	-	M	
aa	X	MT	-	-	MT	MT	-	MT	-	-	-	-	M	
ab	X	M	-	T	MT	MT	-	MT	-	-	-	-	M	
ac	X	MT	-	T	MT	-	-	MT	-	-	-	-	M	
ad	X	MT	-	T	-	-	-	MT	-	-	-	-	M	
ae	X	MT	-	T	-	-	-	MT	-	MT	-	-	M	
af	X	T	-	T	-	-	-	-	-	M	-	-	M	
ag	X	M	-	T	MT	-	-	M	-	T	-	-	M	
ah	XM	M	-	MT	M	MT	-	-	-	-	-	-	M	
ai	X	M	-	MT	MT	-	-	-	-	-	-	-	M	
aj	X	MT	-	MT	MT	-	-	-	-	MT	-	-	M	
ak	XM	MT	MT	M	M	-	-	-	-	MT	-	-	M	
al	X	M	MT	M	M	T	-	-	-	T	-	-	M	
am	M	MT	M	M	M	-	-	-	-	-	-	-	M	
an	MT	MT	MT	M	M	MT	-	-	-	-	-	-	M	
ao	-	-	M	M	M	M	-	-	-	-	-	-	M	
ap	-	-	XM	M	M	M	-	-	-	-	-	-	M	
aq	-	-	M	M	M	M	-	-	-	-	T	-	M	
ar	-	-	M	M	M	M	-	-	MT	-	MT	-	M	
as	X	M	-	M	M	T	-	-	-	T	-	-	M	
at	X	M	-	-	M	-	-	-	-	-	-	-	M	

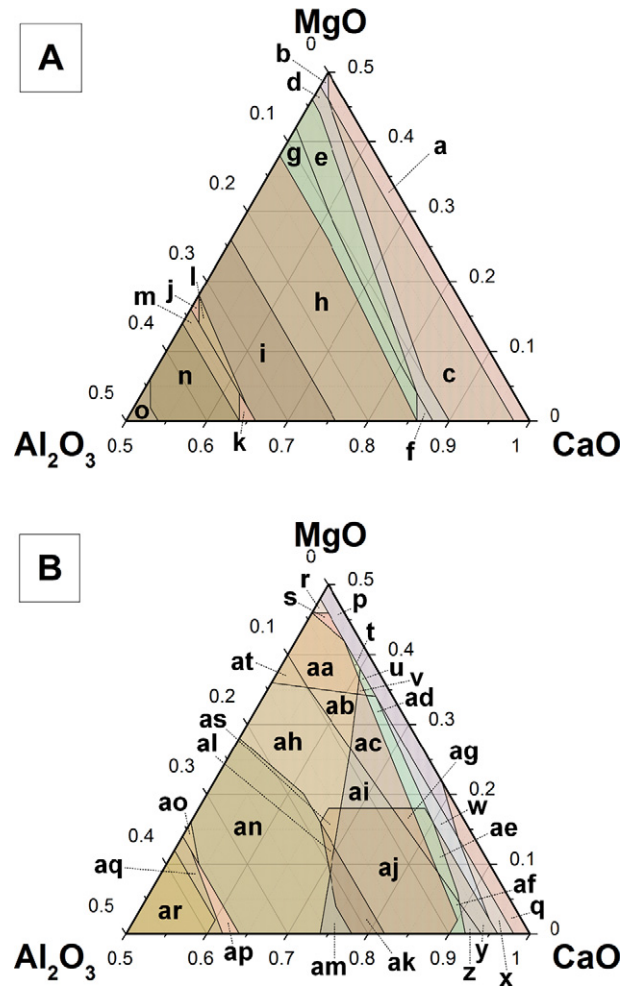


Fig. 3. Phase diagrams in the CaO-Al<sub>2</sub>O<sub>3</sub>-MgO chemical system for N<sup>-</sup>activated slag binders derived from BFS with sulfide at a molar equivalent to 2 wt% SO<sub>3</sub> and A) 30 wt% SiO<sub>2</sub> or B) 40 wt% SiO<sub>2</sub>. The w/b ratio is 0.4, the slag reaction extent is 60%, and the units are in mol fraction. The additional simulated solid phases are: 1, CNASH<sub>ss</sub>; 2, MA-OH-LDH<sub>ss</sub>; 3, strätlingite; 5, ettringite; 7, natrolite; 8, Ca-heulandite; 9, portlandite; 10, brucite; 11, AH<sub>3</sub>(<sub>mc</sub>); 12, C<sub>4</sub>A $\bar{C}$ H<sub>11</sub>; 13, MA- $\bar{C}$ -LDH; 14, calcite. Solid phases are classified by quantity, with major, minor, and trace phases denoted in the legend by X, M, and T, respectively. Multiple letters are used where more than one category applies.

Al LDH phase relative to its carbonate-free counterpart may seem counterintuitive considering the strong thermodynamic preference for this LDH type to intercalate CO<sub>2</sub> [54,55], and the relatively high CO<sub>2</sub> concentration in this N<sup>-</sup>activated slag system at early times of reaction. However, thermodynamic data for MA-OH-LDH phases [25,56,57] that were recently recompiled for improved reliability during the development of the MA-OH-LDH<sub>ss</sub> solid solution model [11] showed that this phase was systematically less soluble than MA- $\bar{C}$ -LDH. The solubility of the carbonate-bearing phase has also recently been reassessed [58,59]. Therefore, more thermodynamic data for Mg-Al-type LDH phases, particularly MA-OH-LDH, are needed to more confidently predict the relative stabilities of these phases in AAS binders.

3.4. Phase diagrams for N<sup>-</sup>activated slag binders

The CNASH<sub>ss</sub> phase is stable over a similar range of CaO-Al<sub>2</sub>O<sub>3</sub>-MgO compositions in the simulated N<sup>-</sup>activated slag binders relative to the other AAS systems modelled above (Al<sub>2</sub>O<sub>3</sub>/(CaO + Al<sub>2</sub>O<sub>3</sub> + MgO) < ~0.33), although the stability of MA-OH-LDH<sub>ss</sub> is slightly reduced in the 30 wt% SiO<sub>2</sub> slag system at low MgO concentrations (Fig. 4A). Ettringite is predicted to stabilise in N<sup>-</sup>activated slag binders, occurring over essentially the full range of modelled

CaO-Al<sub>2</sub>O<sub>3</sub>-MgO compositions (Al<sub>2</sub>O<sub>3</sub>/(CaO + Al<sub>2</sub>O<sub>3</sub> + MgO) > ~0.03). Gypsum is predicted to precipitate only at low-Al compositions, and is slightly more stable in the 40 wt% SiO<sub>2</sub> system. The relatively high stability of these phases in the simulations is consistent with the experimental identification of these phases in binders produced by sodium sulfate activation of BFS [20]. The C<sub>4</sub>A $\bar{C}$ H<sub>ss</sub> phase is only predicted to stabilise at a slag SiO<sub>2</sub> content of 30 wt% and intermediate CaO-Al<sub>2</sub>O<sub>3</sub>-MgO compositions (~0.05 < Al<sub>2</sub>O<sub>3</sub>/(CaO + Al<sub>2</sub>O<sub>3</sub> + MgO) < ~0.25 and CaO/(CaO + Al<sub>2</sub>O<sub>3</sub> + MgO) > ~0.6). This moderate stability regime is consistent with experimentally-determined solid phase assemblages for N<sup>-</sup>activated slag binders which show that the occurrence of this phase depends strongly on the slag chemical composition [20].

Similar trends in phase stability are also simulated for the other stable solid phases in the N<sup>-</sup>activated slag system: strätlingite is more stable at higher Al concentrations (Al<sub>2</sub>O<sub>3</sub>/(CaO + Al<sub>2</sub>O<sub>3</sub> + MgO) > ~0.15) and in the lower SiO<sub>2</sub>-content slag system (Fig. 4A), becoming the major solid phase at the high-Al limit of the simulated composition range; AH<sub>3</sub>(<sub>mc</sub>) only precipitates at very high Al content (Al<sub>2</sub>O<sub>3</sub>/(CaO + Al<sub>2</sub>O<sub>3</sub> + MgO) > ~0.35), portlandite is progressively less stable at higher SiO<sub>2</sub> and lower CaO content, with a very small stability field in the 40 wt% SiO<sub>2</sub> system (Fig. 4B); brucite is stable over the full range of MgO compositions but is progressively destabilised with respect to MA-OH-LDH<sub>ss</sub> at higher Al concentrations; and the relative stabilities of

Region	Simulated solid phase assemblage														
	1	2	3	5	6	7	8	9	10	11	15				
a	X	-	-	-	-	-	-	-	MT	MT	-	M			
b	X	-	-	-	-	-	-	-	-	-	-	-	M		
c	X	-	-	T	-	-	-	-	-	-	-	-	-	-	
d	X	-	-	MT	-	-	-	-	MT	MT	-	-	-	-	
e	X	-	-	MT	MT	-	-	-	MT	MT	-	-	-	-	
f	X	-	-	MT	M	-	-	-	-	-	-	-	-	-	
g	X	-	-	MT	MT	-	-	-	-	MT	-	-	-	-	
h	X	MT	-	MT	-	-	-	-	-	MT	-	-	-	-	
i	X	M	-	MT	-	-	-	-	-	-	-	-	-	-	
j	X	MT	-	MT	MT	-	-	-	-	MT	-	-	-	-	
k	X	MT	-	MT	MT	-	-	-	-	-	-	-	-	-	
l	X	MT	XM	MT	M	-	-	-	-	-	-	-	-	-	
m	XM	M	-	MT	-	MT	-	-	-	-	-	-	-	-	
n	X	M	-	M	MT	T	-	-	-	-	-	-	-	-	
o	XM	MT	XMT	MT	MT	MT	-	-	-	-	-	-	-	-	
p	XM	MT	XMT	MT	-	MT	-	-	-	-	-	-	-	-	
q	MT	MT	XM	MT	-	M	T	-	-	-	-	-	-	-	
r	-	MT	XM	T	-	M	MT	-	-	-	-	-	-	-	
s	-	MT	XM	T	-	M	MT	-	-	-	MT	-	-	-	
t	X	-	-	-	-	-	-	MT	MT	-	MT	-	MT	-	
u	X	-	-	-	-	-	-	MT	MT	-	MT	-	MT	-	
v	X	-	-	T	-	-	MT	-	M	-	MT	-	MT	-	
w	X	-	-	MT	-	-	-	-	-	-	-	-	-	MT	
x	X	-	-	T	-	-	-	-	T	T	-	-	-	T	
y	X	-	-	T	-	-	-	-	T	T	-	-	-	-	
z	MT	-	-	MT	-	-	MT	-	M	-	-	-	-	-	
aa	X	-	-	MT	-	-	-	-	-	MT	-	-	-	-	
ab	X	T	-	-	-	T	-	-	-	-	-	-	-	-	
ac	MT	T	-	MT	-	-	MT	-	MT	-	-	-	-	-	
ad	X	T	-	MT	-	-	-	-	-	T	-	-	-	-	
ae	X	M	-	T	-	T	-	-	-	T	-	-	-	-	
af	MT	MT	-	MT	-	MT	MT	-	-	-	-	-	-	-	
ag	XM	MT	-	MT	-	T	MT	-	MT	-	-	-	-	-	
ah	X	MT	-	T	-	T	-	-	-	-	-	-	-	-	
ai	X	-	-	-	-	-	-	-	-	-	-	-	-	-	
aj	X	T	MT	T	-	MT	-	-	-	-	-	-	-	-	
ak	XMT	MT	MT	MT	-	MT	MT	-	-	-	-	-	-	-	
al	-	MT	M	T	-	M	M	-	-	-	-	-	-	-	
am	-	MT	M	T	-	M	M	-	-	-	MT	-	-	-	

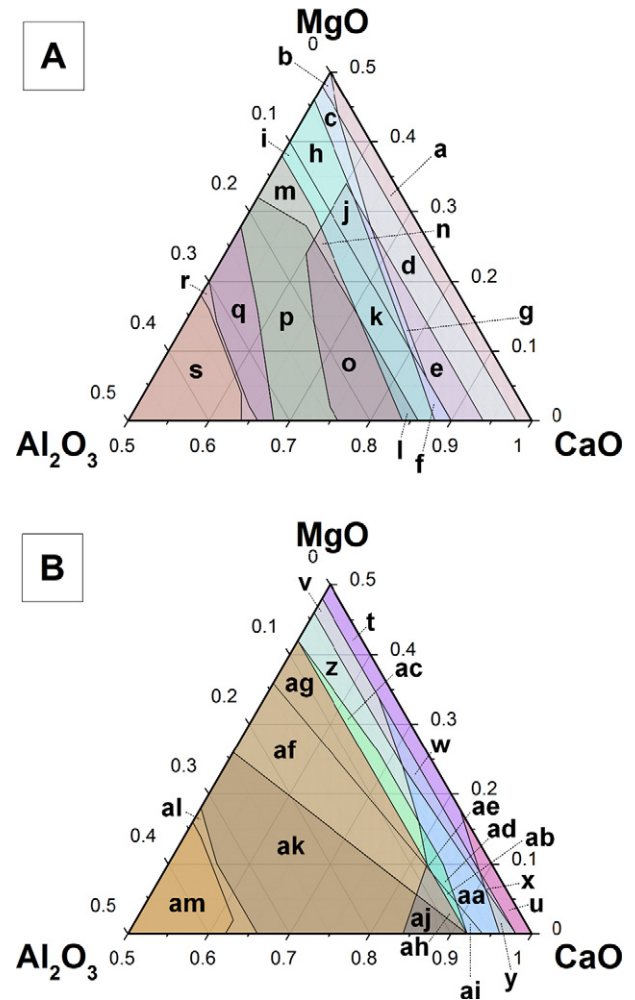


Fig. 4. Phase diagrams in the CaO-Al<sub>2</sub>O<sub>3</sub>-MgO chemical system for NS-activated slag binders derived from BFS with sulfide at a molar equivalent to 2 wt% SO<sub>3</sub> and A) 30 wt% SiO<sub>2</sub> or B) 40 wt% SiO<sub>2</sub>. The w/b ratio is 0.4, the slag reaction extent is 60%, and the units are in mol fraction. The simulated solid phases are: 1, CNASH<sub>ss</sub>; 2, MA-OH-LDH<sub>ss</sub>; 3, strätlingite; 5, ettringite; 6, C<sub>4</sub>A<sub>5</sub>H<sub>3</sub>ss; 7, natrolite; 8, Ca-heulandite; 9, portlandite; 10, brucite; 11, AH<sub>3</sub>(<sub>mc</sub>); 15, gypsum. Solid phases are classified by quantity, with major, minor, and trace phases denoted in the legend by X, M, and T, respectively. Multiple letters are used where more than one category applies.

natrolite and Ca-heulandite are predicted to increase at higher SiO<sub>2</sub> and Al<sub>2</sub>O<sub>3</sub> concentrations.

### 3.5. Aqueous phase chemical compositions

Chemical compositions of the aqueous phases in the simulated AAS binders were simulated to visualise correlations between these data and the predicted solid phase assemblages discussed in Sections 3.1–3.4. The pH is  $\geq 13$  in the bulk chemical composition region most relevant to BFS-activated slag binders (bottom-middle to centre-right of the plots [11]) and is generally lowest at the most Ca-deficient compositions (approaching 11 here), for each simulated system; see Supporting Information. The simulated pH is typically higher in the 30 wt% SiO<sub>2</sub> systems and for NC-activated slag binders, and lower in the NS-activated slag systems.

Dissolved Al concentrations in each of the 30 wt% SiO<sub>2</sub> AAS systems are reproduced here in Fig. 5, with the full set of aqueous phase chemical composition results presented as Supporting Information.

The simulated solid phase assemblages are most strongly correlated with the aqueous Al concentrations (Fig. 5), but other dissolved element concentrations are also sometimes strongly related to the simulated solid phases, e.g., carbon in the NC-activated slag systems,

and sulfur in the NS-activated slag systems. This result is consistent with other experimental and modelling work that has shown that Al is preferentially bound in C-(N)-A-S-H gels in AAS binders, with the remainder incorporated into secondary solid phases such as AFm [15].

## 4. Conclusions

Phase diagrams for NS-, NS<sub>2</sub>-, NC- and NS-activated slag binders were simulated over the pseudo-ternary CaO-Al<sub>2</sub>O<sub>3</sub>-MgO composition region relevant to these materials. The simulation results were consistent with the common experimental observation that C-(N)-A-S-H gel and Mg-Al LDH phases are the dominant phases formed in these materials. Relationships between the stabilities of the other major, minor, and trace solid reaction products and chemical compositions were identified. Strätlingite was shown to be stabilised at relatively low to intermediate Si concentrations and at high Al content, contrasting with the stabilities of zeolites, which tend to stabilise at both higher Si and Al concentrations. Katoite and AFm-type phases were found to stabilise at intermediate CaO-Al<sub>2</sub>O<sub>3</sub>-MgO compositions. The modelled solid phase assemblages were closely correlated to aqueous Al concentrations. Therefore, the simulations are in good overall agreement with the experimental literature for AAS materials and advance the precision

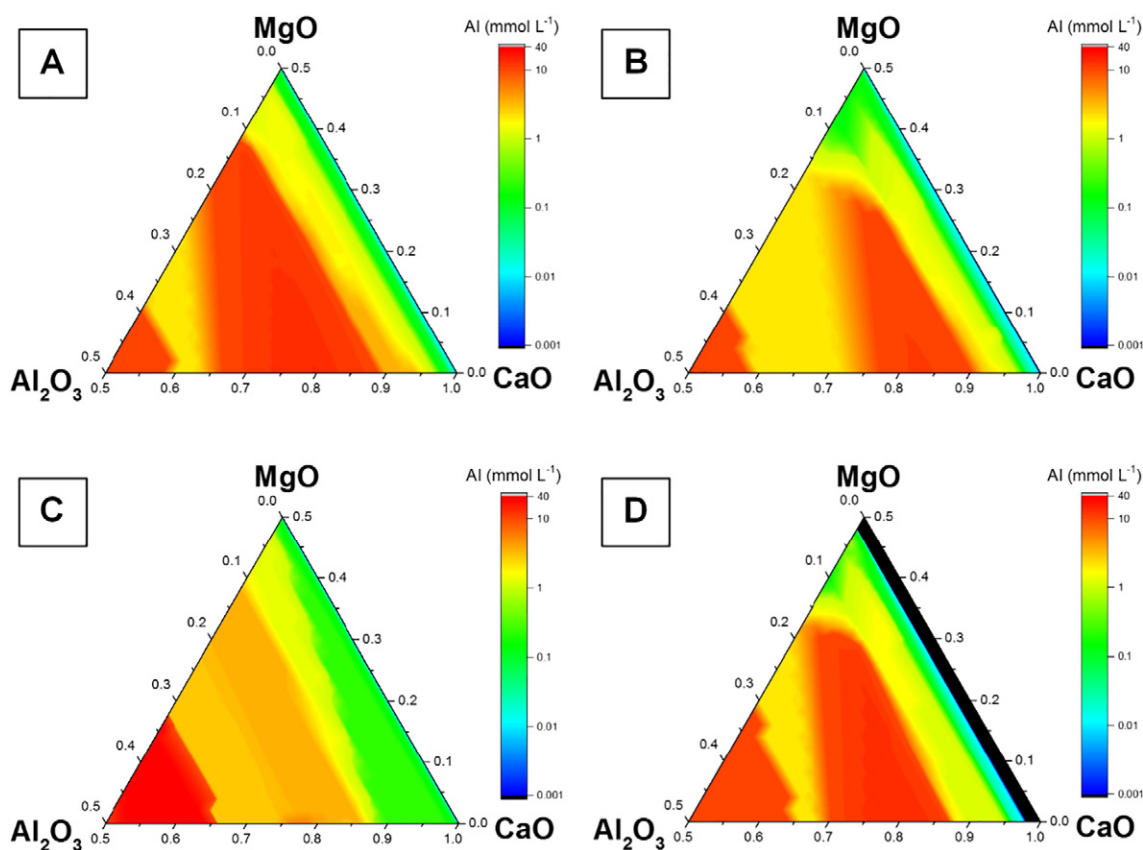


**Fig. 5.** Simulated aqueous Al concentrations in the CaO-Al<sub>2</sub>O<sub>3</sub>-MgO chemical system for A) NS-, B) NS<sub>2</sub>-, C) NC<sup>-</sup>, and D) NS<sup>-</sup>-activated slag binders derived from BFS with sulfide at a molar equivalent to 2 wt% SO<sub>3</sub> and 30 wt% SiO<sub>2</sub>. The w/b ratio is 0.4, the slag reaction extent is 60%, and the units are in mol fraction. The black shaded regions represent Al concentrations <0.001 mmol L<sup>-1</sup>.

with which AAS binders can be designed with respect to solid phase assemblages and related chemical properties.

### Conflict of interest

The authors declare no competing financial interests.

### Acknowledgements

The research of R. J. Myers was funded by The University of Sheffield, Siam Cement Public Company (SCG) Ltd. at the University of California, Berkeley, and is funded by National Science Foundation Grant #1636509 at Yale University. The participation of J. L. Provis and S. A. Bernal in this study is funded by the European Research Council under the European Union's Seventh Framework Programme (FP7/2007-2013)/ERC Grant Agreement #335928 (GeopolyConc).

### Appendix A. Supplementary data

Supplementary data to this article can be found online at <http://dx.doi.org/10.1016/j.cemconres.2017.02.006>.

### References

- [1] H. Xu, J.L. Provis, J.S.J. van Deventer, P.V. Krivenko, Characterization of aged slag concretes, *ACI Mater. J.* 105 (2008) 131–139.
- [2] J.L. Provis, J.S.J. van Deventer (Eds.), *Alkali-Activated Materials, State-Of-The-Art Report*, RILEM TC 244-AAM, Springer/RILEM, Dordrecht, Netherlands, 2014.
- [3] A.O. Purdon, The action of alkalis on blast-furnace slag, *J Soc Chem Ind Trans Commun* 59 (1940) 191–202.
- [4] C. Shi, J. Qian, High performance cementing materials from industrial slags - a review, *Resour. Conserv. Recycl.* 29 (2000) 195–207.
- [5] Y. Bai, N.C. Collier, N.B. Milestone, C.H. Yang, The potential for using slags activated with near neutral salts as immobilisation matrices for nuclear wastes containing reactive metals, *J. Nucl. Mater.* 413 (2011) 183–192.
- [6] R.J. Myers, S.A. Bernal, J.L. Provis, J.D. Gehman, J.S.J. van Deventer, The role of Al in cross-linking of alkali-activated slag cements, *J. Am. Ceram. Soc.* 98 (2015) 996–1004.
- [7] M. Ben Haha, G. Le Saoût, F. Winnefeld, B. Lothenbach, Influence of activator type on hydration kinetics, hydrate assemblage and microstructural development of alkali activated blast-furnace slags, *Cem. Concr. Res.* 41 (2011) 301–310.
- [8] S.D. Wang, K.L. Scrivener, Hydration products of alkali activated slag cement, *Cem. Concr. Res.* 25 (1995) 561–571.
- [9] F. Bonk, J. Schneider, M.A. Cincotto, H. Panepucci, Characterization by multinuclear high-resolution NMR of hydration products in activated blast-furnace slag pastes, *J. Am. Ceram. Soc.* 86 (2003) 1712–1719.
- [10] F. Puertas, M. Palacios, H. Manzano, J.S. Dolado, A. Rico, J. Rodríguez, A model for the C-A-S-H gel formed in alkali-activated slag cements, *J. Eur. Ceram. Soc.* 31 (2011) 2043–2056.
- [11] R.J. Myers, B. Lothenbach, S.A. Bernal, J.L. Provis, Thermodynamic modelling of alkali-activated slag cements, *Appl. Geochem.* 61 (2015) 233–247.
- [12] A.R. Brough, A. Atkinson, Sodium silicate-based, alkali-activated slag mortars - part I. Strength, hydration and microstructure, *Cem. Concr. Res.* 32 (2002) 865–879.
- [13] O. Burciaga-Díaz, J.I. Escalante-García, Structure, mechanisms of reaction, and strength of an alkali-activated blast-furnace slag, *J. Am. Ceram. Soc.* 96 (2013) 3939–3948.
- [14] S.A. Bernal, R. San Nicolas, R.J. Myers, R. Mejía de Gutiérrez, F. Puertas, J.S.J. van Deventer, J.L. Provis, MgO content of slag controls phase evolution and structural changes induced by accelerated carbonation in alkali-activated binders, *Cem. Concr. Res.* 57 (2014) 33–43.
- [15] M. Ben Haha, B. Lothenbach, G. Le Saoût, F. Winnefeld, Influence of slag chemistry on the hydration of alkali-activated blast-furnace slag - part II: effect of Al<sub>2</sub>O<sub>3</sub>, *Cem. Concr. Res.* 42 (2012) 74–83.
- [16] S.A. Bernal, J.L. Provis, R.J. Myers, R. San Nicolas, J.S.J. van Deventer, Role of carbonates in the chemical evolution of sodium carbonate-activated slag binders, *Mater. Struct.* 48 (2015) 517–529.
- [17] X. Ke, S.A. Bernal, J.L. Provis, Controlling the reaction kinetics of sodium carbonate-activated slag cements using calcined layered double hydroxides, *Cem. Concr. Res.* 81 (2016) 24–37.

- [18] S.A. Bernal, Advances in near-neutral salts activation of blast furnace slags, RILEM Tech Lett 1 (2016) 39–44.
- [19] L.G. Baquerizo, T. Matschei, K.L. Scrivener, M. Saeidpour, L. Wadsö, Hydration states of AFm cement phases, Cem. Concr. Res. 73 (2015) 143–157.
- [20] S.A. Bernal, X. Ke, J.L. Provis, Activation of Slags Using Near-Neutral Salts: The Importance of Slag Chemistry, in: Proceedings of the 14th International Congress on the Chemistry of Cement/Beijing 2015.
- [21] R.J. Myers, S.A. Bernal, J.L. Provis, A thermodynamic model for C-(N)-A-S-H gel: CNASH<sub>ss</sub>. Derivation and application, Cem. Concr. Res. 66 (2014) 27–47.
- [22] R.J. Myers, B. Lothenbach, S.A. Bernal, J.L. Provis, Corrigendum to “Thermodynamic modelling of alkali-activated slag-based cements” [Appl. Geochem. 61 (2015) 233–247], Appl. Geochem. 67 (2016) 186.
- [23] B. Lothenbach, A. Gruskovnjak, Hydration of alkali-activated slag: thermodynamic modelling, Adv. Cem. Res. 19 (2007) 81–92.
- [24] B. Lothenbach, T. Matschei, G. Möschner, F.P. Glasser, Thermodynamic modelling of the effect of temperature on the hydration and porosity of Portland cement, Cem. Concr. Res. 38 (2008) 1–18.
- [25] D.G. Bennett, D. Read, M. Atkins, F.P. Glasser, A thermodynamic model for blended cements. II: cement hydrate phases; thermodynamic values and modelling studies, J. Nucl. Mater. 190 (1992) 315–325.
- [26] C. Shi, P.V. Krivenko, D. Roy, Alkali-Activated Cements and Concretes, first ed. Taylor & Francis, New York, 2006.
- [27] E.F. Osborn, K.H. Gee, A. Muan, P.L. Roeder, G.C. Ulmer, 1. Phase equilibria at solidus temperatures in the quaternary system CaO-MgO-Al<sub>2</sub>O<sub>3</sub>-SiO<sub>2</sub> and their bearing on optimum composition of blast furnace slag and on slag properties, Bulletin of the Earth and Mineral Sciences Experiment Station, 85, The Pennsylvania State University, University Park, 1969.
- [28] S.A. Bernal, V. Rose, J.L. Provis, The fate of iron in blast furnace slag particles during alkali-activation, Mater. Chem. Phys. 146 (2014) 1–5.
- [29] D.A. Kulik, T. Wagner, S.V. Dmytrieva, G. Kosakowski, F.F. Hingerl, K.V. Chudnenko, U. Berner, GEM-Selektor geochemical modeling package: revised algorithm and GEMS3K numerical kernel for coupled simulation codes, Comput. Geosci. 17 (2013) 1–24.
- [30] T. Wagner, D.A. Kulik, F.F. Hingerl, S.V. Dmytrieva, GEM-Selektor geochemical modeling package: TSolMod library and data interface for multicomponent phase models, Can. Mineral. 50 (2012) 1173–1195.
- [31] A. Dauzeres, G. Achiedo, D. Nied, E. Bernard, S. Alahrache, B. Lothenbach, Magnesium perturbation in low-pH concretes placed in clayey environment—solid characterizations and modeling, Cem. Concr. Res. 79 (2016) 137–150.
- [32] D. Nied, K. Enemark-Rasmussen, E. L'Hopital, J. Skibsted, B. Lothenbach, Properties of magnesium silicate hydrates (M-S-H), Cem. Concr. Res. 79 (2016) 323–332.
- [33] H.C. Helgeson, D.H. Kirkham, G.C. Flowers, Theoretical prediction of the thermodynamic behavior of aqueous electrolytes at high pressures and temperatures: IV. Calculation of activity coefficients, osmotic coefficients, and apparent molal and standard and relative partial molal properties to 600°C and 5 kb, Am. J. Sci. 281 (1981) 1249–1516.
- [34] R.J. Myers, S.A. Bernal, R. San Nicolas, J.L. Provis, Generalized structural description of calcium-sodium aluminosilicate hydrate gels: the cross-linked substituted tobermorite model, Langmuir 29 (2013) 5294–5306.
- [35] R. Barbarulo, H. Peycelon, S. Leclercq, Chemical equilibria between C-S-H and ettringite, at 20 and 85 °C, Cem. Concr. Res. 37 (2007) 1176–1181.
- [36] Y. Fu, P. Xie, P. Gu, J.J. Beaudoin, Effect of temperature on sulphate adsorption/desorption by tricalcium silicate hydrates, Cem. Concr. Res. 24 (1994) 1428–1432.
- [37] F.L. Theiss, S.J. Palmer, G.A. Ayoko, R.L. Frost, Sulfate intercalated layered double hydroxides prepared by the reformation effect, J. Therm. Anal. Calorim. 107 (2012) 1123–1128.
- [38] T. Matschei, B. Lothenbach, F.P. Glasser, Thermodynamic properties of Portland cement hydrates in the system CaO-Al<sub>2</sub>O<sub>3</sub>-SiO<sub>2</sub>-CaSO<sub>4</sub>-CaCO<sub>3</sub>-H<sub>2</sub>O, Cem. Concr. Res. 37 (2007) 1379–1410.
- [39] D. Peak, Adsorption mechanisms of selenium oxyanions at the aluminum oxide/water interface, J. Colloid Interface Sci. 303 (2006) 337–345.
- [40] M.U. Okoronkwo, F.P. Glasser, Stability of strätlingite in the CASH system, Mater. Struct. 49 (2016) 4305–4318.
- [41] I.G. Richardson, G.W. Groves, Microstructure and microanalysis of hardened cement pastes involving ground granulated blast-furnace slag, J. Mater. Sci. 27 (1992) 6204–6212.
- [42] S.A. Bernal, J.L. Provis, V. Rose, R. Mejía De Gutierrez, Evolution of binder structure in sodium silicate-activated slag-metakaolin blends, Cem. Concr. Compos. 33 (2011) 46–54.
- [43] J. Schneider, M.A. Cincotto, H. Panepucci, <sup>29</sup>Si and <sup>27</sup>Al high-resolution NMR characterization of calcium silicate hydrate phases in activated blast-furnace slag pastes, Cem. Concr. Res. 31 (2001) 993–1001.
- [44] I.G. Richardson, A.R. Brough, G.W. Groves, C.M. Dobson, The characterization of hardened alkali-activated blast-furnace slag pastes and the nature of the calcium silicate hydrate (C-S-H) phase, Cem. Concr. Res. 24 (1994) 813–829.
- [45] F. Puertas, M. Palacios, T. Vázquez, Carbonation process of alkali-activated slag mortars, J. Mater. Sci. 41 (2006) 3071–3082.
- [46] W. Hummel, U. Berner, E. Curti, F.J. Pearson, T. Thoenen, Nagra/PSI Chemical Thermodynamic Database 01/01, Universal Publishers, Parkland, Florida, 2002.
- [47] T. Thoenen, W. Hummel, U. Berner, The PSI/Nagra chemical thermodynamic database 12/07: present status and future developments, Mineral. Mag. 77 (2013) 2327.
- [48] H.C. Helgeson, J.M. Delany, H.W. Nesbitt, Summary and critique of the thermodynamic properties of rock-forming minerals, Am. J. Sci. 278-A (1978) 1–229.
- [49] B. Lothenbach, F. Winnefeld, Thermodynamic modelling of the hydration of Portland cement, Cem. Concr. Res. 36 (2006) 209–226.
- [50] F.P. Glasser, The stability of ettringite, in: K.L. Scrivener, J.A.N. Skalny (Eds.), International RILEM Workshop on Internal Sulfate Attack and Delayed Ettringite Formation, RILEM Publications SARL, Villars, Switzerland, 2004.
- [51] B. Lothenbach, G. Le Saout, E. Gallucci, K. Scrivener, Influence of limestone on the hydration of Portland cements, Cem. Concr. Res. 38 (2008) 848–860.
- [52] A.R. Sakulich, S. Miller, M.W. Barsoum, Chemical and microstructural characterization of 20-month-old alkali-activated slag cements, J. Am. Ceram. Soc. 93 (2010) 1741–1748.
- [53] J.W. Morse, R.S. Arvidson, A. Lüttge, Calcium carbonate formation and dissolution, Chem. Rev. 107 (2007) 342–381.
- [54] R. Allada, A. Navrotsky, J. Boerio-Goates, Thermochemistry of hydrotalcite-like phases in the MgO-Al<sub>2</sub>O<sub>3</sub>-CO<sub>2</sub>-H<sub>2</sub>O system: a determination of enthalpy, entropy, and free energy, Am. Mineral. 90 (2005) 329–335.
- [55] R.K. Allada, J.D. Pless, T.M. Nenoff, A. Navrotsky, Thermochemistry of hydrotalcite-like phases intercalated with CO<sub>3</sub><sup>2-</sup>, NO<sub>3</sub><sup>-</sup>, Cl<sup>-</sup>, I<sup>-</sup>, and ReO<sub>4</sub><sup>-</sup>, Chem. Mater. 17 (2005) 2455–2459.
- [56] K. Morimoto, S. Anraku, J. Hoshino, T. Yoneda, T. Sato, Surface complexation reactions of inorganic anions on hydrotalcite-like compounds, J. Colloid Interface Sci. 384 (2012) 99–104.
- [57] W. Gao, Z. Li, Solubility and K<sub>sp</sub> of Mg<sub>4</sub>Al<sub>2</sub>(OH)<sub>14</sub>·3H<sub>2</sub>O at the various ionic strengths, Hydrometallurgy 117–118 (2012) 36–46.
- [58] K.B. Rozov, U. Berner, D.A. Kulik, L.W. Diamond, Solubility and thermodynamic properties of carbonate-bearing hydrotalcite-pyroaurite solid solutions with a 3:1 Mg/(Al+Fe) mole ratio, Clay Clay Miner. 59 (2011) 215–232.
- [59] C.A. Johnson, F.P. Glasser, Hydrotalcite-like minerals (M<sub>2</sub>Al(OH)<sub>6</sub>(CO<sub>3</sub>)<sub>0.5</sub>·XH<sub>2</sub>O, where M=Mg, Zn, Co, Ni) in the environment: synthesis, characterization and thermodynamic stability, Clay Clay Miner. 51 (2003) 1–8.